Journal of Energy Storage 30 (2020) 101552

Contents lists available at ScienceDirect

Journal of Energy Storage

journal homepage: www.elsevier.com/locate/est

Prediction of constant power delivery of lithium-ion cells at high loads

Christoph Nebl[a], Frank-Oliver Kotzur[b], Daniel Koch[a], Hans-Georg Schweiger[a,*]

[a] Technische Hochschule Ingolstadt (THI), Esplanade 10, 85049 Ingolstadt, Germany
[b] AVL Deutschland GmbH, Marie-Curie-Str. 1, 85055 Ingolstadt, Germany

ARTICLE INFO

Keywords:
Constant power discharge
Lithium-ion batteries
Peukert equation
High load amplitudes
Constant power prediction
Discharge power

ABSTRACT

Available energy and available capacity are key factors for dimensioning batteries. Discharge duration of a battery and its dependency on discharge current amplitude are well described by Peukert's law from low to medium current ranges. Other equations describe this dependency up to very high current rates, including the currents occurring during a short circuit. It is not current and capacity, but energy and power which are the key parameters for dimensioning battery systems. Thus, the available power of battery cells, vs. the discharge duration was investigated from low to high constant power discharge loads. Based on the results of these experiments, a correlation of the maximum discharge duration for low to medium discharge power pulses, similar to the Peukert's equation was found. Additionally, a new equation is proposed, describing the power range from low to very high discharge power rates.

The result of this work simplifies the design of battery systems, its electromechanical components, as well as improves the prediction of available boost power cost-effective way e.g. for hybrid electric vehicles.

1. Introduction

A good understanding to manufacturers and consumers of battery cells and systems about the dynamic behavior of their energy storage systems especially of the peak discharge power capability of lithium-ion-batteries is crucial for safe and reliable operation of hybrid and electric vehicles. Particularly if the electric power train is used to provide active yaw control of the vehicle [1]. A sound understanding of the peak charge power of the battery is also necessary, especially in the case of the recuperation of energy into the battery, e.g. to provide safe and reliable distribution of the breaking power between the electric machine and the mechanical brakes [2,3]. Therefore, the prediction of the maximum charge and discharge power of a BEV and HEV for short and high electric loads is important for safe vehicle operation [4].

The power or current a battery system can deliver at low to medium current loads, e. g. discharge loads from 0.8 to 1.5 Watt per cell, can be described by equivalent circuit models [5]. Due to the nonlinear behavior of batteries, these models fail at high discharge loads [6]. To solve this dilemma a good description or model describing the peak power of batteries is needed.

2. Theoretical background

The maximum capacity which can be withdrawn from a battery at medium current loads is described by the well-known Peukert equation [7]:

$$\boldsymbol{I^k \cdot t = Q_p} \tag{1}$$

and

$$t_1(I_1) = \frac{Q_{ra}}{I_{ra}} \cdot \left(\frac{I_{ra}}{I_1}\right)^k \tag{2}$$

Eq. (1) can be expanded for high current loads, e.g. beyond the operation range given in the batteries' data sheet [9,8]. This will lead to the Peukert-bend equation, describing a capacity declining effect at high current loads [9],

$$t_1(I_1) = \frac{Q_{ra}}{I_{ra}} \cdot \left(\frac{I_{ra}}{1\,A}\right)^{k_2} \cdot \left(\frac{1\,A}{I_1}\right)^{k_2} \cdot \sqrt{\frac{1}{s_1\left(\frac{I_1}{s_2}-1\right)+1}} \tag{3}$$

Both equations describe the amount of charge which can be withdrawn from the cell as well the maximum discharge duration. Table 1 explains the symbols used in Eq. (1–3).

Q_{ra} is the nominal capacity at the rated discharge current I_{ra}, which is specified by the manufacturer. t_1 is the calculated discharge time at the discharge current I_1, which is the main benefit of Eq. (3).

The parameter s_1 characterizes the intensity of the capacity decrease and s_2 is a dimensionless value on which the fitting of Eq. (3) deviates

* Corresponding author.
E-mail address: Hans-Georg.Schweiger@thi.de (H.-G. Schweiger).

https://doi.org/10.1016/j.est.2020.101552
Received 12 November 2019; Received in revised form 28 January 2020; Accepted 12 May 2020
Available online 28 May 2020
2352-152X/ © 2020 The Authors. Published by Elsevier Ltd. This is an open access article under the CC BY-NC-ND license (http://creativecommons.org/licenses/BY-NC-ND/4.0/).

Table 1
Symbols corresponding to Eqs. (1–3).

ra	Rated cell capacity (nominal)
Q_p	Battery capacity at 1 A discharge current
t_1	Calculated discharge time
T	Discharge time at 1 A discharge current
I	1 A discharge current
I_1	Chosen discharge current
I_{ra}	Rated discharge current (nominal)
k, k_2	Peukert exponent (fitting parameter)
s_1	Peukert bend fitting parameter
s_2	Peukert bend fitting parameter

Table 2
Symbols referring to Eqs. (4–6).

T	Discharge time
E	Discharge energy
U	Actual voltage
I	Discharge current
E	Available energy at 1 W discharge power
K	Peukert similar exponent (fitting parameter)
E_{ra}	Rated energy at rated discharge power (nominal)
P_{ra}	Rated power at nominal energy determination
P_1	Chosen constant discharge power

more than the gain factor $\frac{1}{\sqrt{2}}$ (similar to the cut-off frequency of electronic filters) of the classic Peukert equation [7,9].

To get the results for Eq. (3), the constant current measuring method needs to be applied. For the new prediction of the constant power delivery in this work, the constant power test method was used.

Fig. 1 shows the difference between the two measurement methods, constant current (Fig. 1a, 22.0 A / $\bar{P}$ = 68.0 W) and constant power (Fig. 1b, 60.0 W) discharge. The power characteristic of both test methods become apparent.

3. Methodology

3.1. Low power behavior

Peukert's law [7] allows one to calculate the discharge time and the extracted charge at a constant discharge current, as introduced in section II. In contrast, in this work a constant discharge power P is of interest.

Generally for the discharge energy E applies:

$$E = U \cdot I \cdot t = constant \tag{4}$$

with U the actual voltage, I the discharge current and the discharge time t.

Analogous to Peukert's law equation (1) the relation

$$t \cdot P^k = E = constant \tag{5}$$

permits a better description of the relation of discharge power P and discharge energy E. Thereby E is the electric energy extracted from the battery at a *1 W* constant power discharge, t is the time in hours the battery needs to be discharged and k is a dimensionless parameter similar to the well-known Peukert exponent.

Analogous to the Peukert equation (1), Eq. (5) is only valid for a standard discharge power of *1 W* instead of *1 A*. If the maximum discharge time as function of the power *t(P)* of the specimen should be determined for any discharge powers, Eq. (5) must be transformed into the following form:

$$t(P_1) = \frac{E_{ra}}{P_{ra}} \cdot \left(\frac{P_{ra}}{P_1}\right)^k = \frac{E_{ra}}{P_{ra}} \cdot \left(\frac{P_{ra}}{1\ W}\right)^k \cdot \left(\frac{1\ W}{P_1}\right)^k \tag{6}$$

This equation corresponds to the low power range of all tested cell types, shown as the linear curve marked in blue in the Figs. 4–7. If the cell voltage is approximated as a constant, Eq. (6) describes the behavior in the low-power region analogous to Peukert's equation for charge and current. Table 2 explains the symbols used in Eq. (4–6).

4. High power behavior

For high discharge powers, significant deviation to the linear low power range become apparent. Similar to the Peukert-bend [1], introduced in Eq. (3), the behavior of the cell during the discharge with constant power can be described. To derive a suitable equation with the necessity to consider a higher declining factor, a similarity to an increased order of low-pass filters was assumed.

The parameter k_1 (Eq. (7)) describes the theoretical energy content of the cell at constant low power discharges and is formed from the first part of Eq. (6), whereby the Peukert exponent k has been renamed to k_2 in Eq. (8-10) to distinguish it:

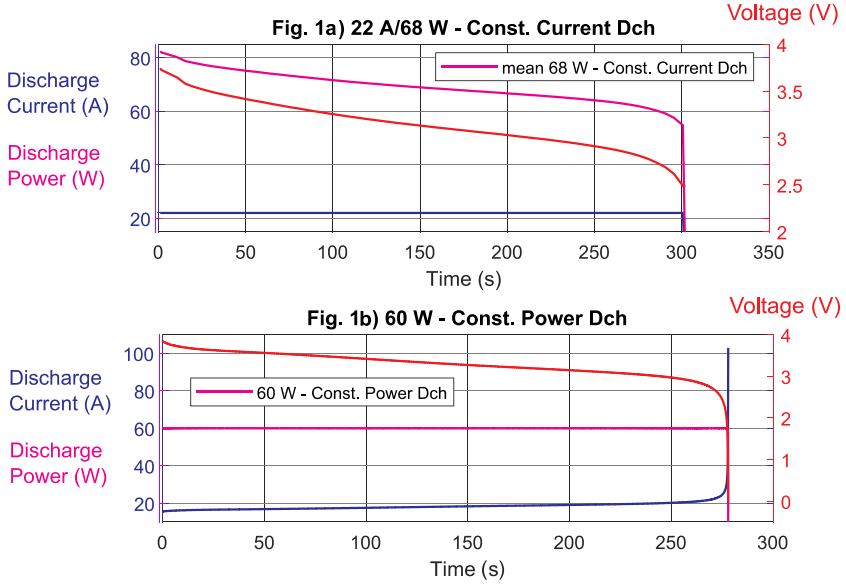

Fig. 1. Current, voltage and power profiles comparison of constant current and constant power discharge.

$$k_1 = \frac{E_{ra}}{P_{ra}} \cdot \left(\frac{P_{ra}}{1\ W}\right)^{k_2} \tag{7}$$

Extending Eq. (6) for constant high-power discharges using Eq. (7) and the described assumption leads to the following relationship:

$$t(P_1) = k_1 \cdot \left(\frac{1\ W}{P_1}\right)^{k_2} \cdot 6 \sqrt{\frac{1}{s_1^{\left(\frac{P_1}{s_2}-1\right)} + 1}} \tag{8}$$

Which can be further transformed into Eq. (9)

$$t(P_1) = \frac{E_{ra}}{P_{ra}} \cdot \left(\frac{P_{ra}}{1\ W}\right)^{k_2} \cdot \left(\frac{1\ W}{P_1}\right)^{k_2} \cdot 6 \sqrt{\frac{1}{s_1^{\left(\frac{P_1}{s_2}-1\right)} + 1}} \tag{9}$$

and describes the relationship between discharge time *t(P)* as function of the discharge power P_1.

Parameter k_1, is the maximum theoretical energy content of the cell for the constant power discharges. The second part of Eq. (9) with the parameter s_2 corresponds to the characteristic power when the extended Eq. (6) deviates more than the gain factor $\frac{1}{\sqrt[6]{2}}$ (about 11 %) from the classical linear Peukert equation.

Figs. 4–7 demonstrate that Eq. (9) delivers a highly suitable fitting approach including the declining area, the high power range, plotted in red. This could be demonstrated with all tested specimens.

The increase of the slope to sixth order was necessary as at high constant power discharge the available discharge time drops much more than for constant discharge currents due to the superimposed voltage curve, the voltage cannot be assumed to be constant. Table 3 explains the symbols used in Eq. (7–9).

Table 3
Symbols referring to Eqs. (7–9).

E_{ra}	Rated energy (nominal)
$t(P_1)$	Discharge time as function of the chosen discharge power
P_{ra}	Rated power at nominal energy determination
P_1	Chosen constant discharge power
k_1	Calculated energy content
k_2	Peukert similar exponent (fitting parameter)
s_1	Fitting parameter
s_2	Fitting parameter

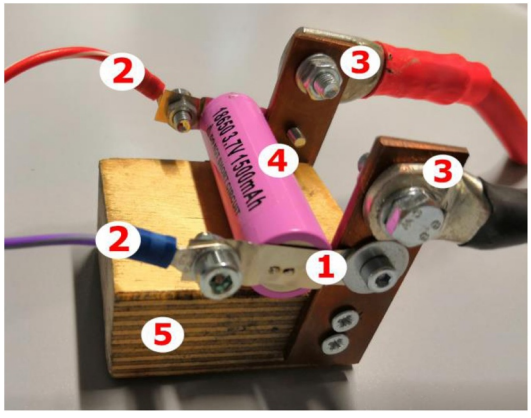

Fig. 2. Test assembly and cell bonding – 1 Nickel-strip, 2 Sense connection, 3 Busbar power connection, 4 battery cell, 5 wooden cell holder.

5. Experimental

5.1. Experimental setup

A Bitrode MCV4-100-5 CE electric vehicle battery cell tester (Bitrode Corporation, St. Louis, USA) test bench was used for the cell tests. It provides eight channels from -100.0 A discharge to 100.0 A charge current and -5.00 V to +5.00 V voltage range. It provides a voltage and current accuracy of ± 0.1 % full-scale.

For reproducible test conditions, all tests were performed in a temperature chamber VT 4021-S, (Weiss Umwelttechnik GmbH, Reiskirchen, Germany) [10]. The chamber is able to cover a temperature range of -40.0 °C to +180.0 °C. A ZENNIUM electrochemical workstation combined with the power potentiostat PP241 (ZAHNER-elektrik GmbH & Co. KG, Kronach, Germany) was used to classify the tested cells by electrochemical impedance spectroscopy (EIS) to reuse them for further investigations, if not aged.

Cells were connected via Kelvin connection to the cell tester. Force connection was implemented by bus bars screwed to Nickel strips which were directly welded to the cells. Sense lines were screwed on the opposite side of the Nickel strips. Fig. 2 implies the described wiring was mounted on a wooden cell holder to relieve the cell of the weight of the cables.

Lithium-ion cells used for the experiments (Table 4):

6. Experimental design

The measurements are based on the standards IEC 61960:2011 [15] and ISO 12405-1:2011 [16].

The lower cut-off voltage was extended to 0.00 V to investigate short-circuit behavior of the battery. This voltage range is important in worst-case considerations for safety-relevant emergency operation of energy storage devices, e.g. for aviation or in road transport for braking systems for electromobility.

6.1. Initial cycles

To ensure stable and reproducible conditions for the subsequent testing, five full discharge/charge cycles were applied to the cells. This completed the basic formation of the cell.

1) Before the test, the cell was left for a reset of at least one hour inside the temperature chamber. The chamber was set to constant temperature of 25.0°C ± 0.5°C. This ensured a homogeneous temperature distribution within the cell. The cell remained inside the temperature chamber for all the subsequent procedures.
2) Complete discharge of the cell with a constant current of 2.0 C until the minimum voltage stated by the cell manufacturer, was reached. Discharge capacity Q was determined by integration of current during the constant current phase of the discharge phase.
3) Recharging of the cell with the constant current constant voltage method (CC-CV) until the maximum cell voltage was reached.

Table 4
Specifications of the tested lithium-ion cells.

Battery Manufacturer/Model	Capacity (Ah)	Discharge current (A)	Cell chemistry	Source
1) LG/ 18650-HB6	1.5	20.0	$LiNiCoMnO_2$	[11]
2) Panasonic/ NCR18650B	3.4	6.2	$LiNiCoAlO_2$	[12]
3) Shenzhen/ IFR18650	1.5	4.5	$LiFePO_4$	[13]
4) Efest/ IMR18650	3.1	20.0	$LiMn_2O_4$	[14]

Current was set to 1.0 C during the constant current phase. The constant voltage phase ended at 0.1 A. Current and cut-off voltage are set according to the specification of the cell manufacturer.
4) Steps 2 and 3 were repeated at least five times until a stable value of the discharge capacity was reached (delta to previous cycles < 3 %). A new cycle was started when the cell had reached a temperature of 25.0°C ± 0.5°C. Due to the low charging current within the CV-phase no additional cooling phases were necessary.
5) Initial cycling was stopped if the < 3 % criteria was reached for the last three cycles of the five initial cycles. For all specimens five runs were sufficient.

7. Measurement cycles

After initial cycling, the cell had a SOC of 100 % due to step 3 in the previous section. The following procedure was used to determine the capability to deliver a constant power until 0.00 V was reached. Fig. 3 shows the flow chart of this test procedure.

1) After the cell was preconditioned, it had an SOC of 100 %. After charging, a temperature equilibrium phase of at least one hour was set to ensure a temperature of 25.0 °C ± 0.5 °C before the test started.
2) Within the power test, the cell was discharged with a constant power regime, until 0.00 V cell voltage was reached. Current and voltage were controlled by the battery tester so a constant discharge power was observed.
3) To avoid heating up the cell during the experiment, another temperature equilibrium phase of 1 hour was set. After this phase the cell temperature was 25.0 °C ± 0.5 °C.
4) Recharging equal to step 3) of the initial cycles (Fig. 3). To detect potential aging of the cell during the measurement cycle, an EIS of the cells was recorded after step 4).
5) In order to eliminate faulty cells or highly aberrant cells, each selected load power was repeated at least three times with new cells of the same type. To be able to exclude systematic errors due to a systematically increasing load sequence of the test specimens, the test sequence of the discharge performances was chosen randomly during the test repetitions.

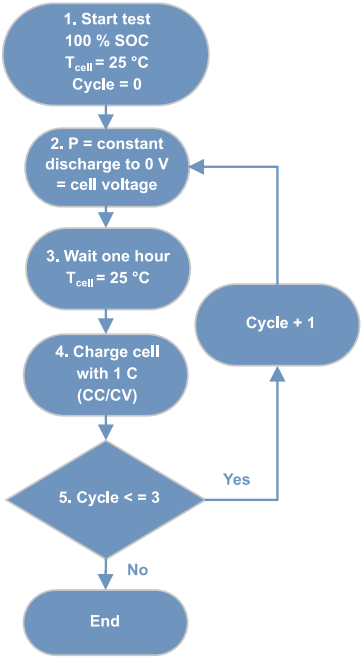

Fig. 3. Main measurement cycle constant power test.

7.1. Cell aging verification for reusage

The impedance spectrum derived from the EIS can change because of many influencing factors. Hence, a comparison between the spectrum of a cell after the main measurements with its spectrum recorded after initial cycling is more meaningful, when it comes to detect aging. The aging information obtained from the repeated recording of the spectra is used for this purpose. The following simple method is used, which does not require any pre-processing of the spectra [17]:

$$\Delta \underline{Z}(j\omega, t) = \underline{Z}(j\omega, t_0) - \underline{Z}(j\omega, t) \tag{10}$$

with t as the time of the measurement, the spectrum was recorded and t_0 as the time of the first measurement after the initial cycles.

To avoid aging effects distorting the results of this work and no aged cells are reused, the impedance spectra were recorded after finishing the third main measurement test run using the Zahner workstation [18]. The checks are compared in accord with Eq. (4) and executed with the following parameters and condition values (Table 5):

$$\Delta\eta = \left(1 - \frac{\underline{Z}(j\omega, t_0)}{\underline{Z}(j\omega, t)}\right) \cdot 100 \tag{11}$$

It was assumed that a cell may be used for further tests (up to a total of three outputs) if the percentage deviation $\Delta\eta$ (Eq. (11)) in relation to the new condition of the battery cell is less than 10 %.

7.2. Conducted discharge power tests

The model 18650-HB6 from LG was tested with the discharge powers 20.0, 30.0, 40.0, 50.0, 60.0, 72.0, 90.0, 108.0, 126.0, 135.0, 144.0, 153.0, 162.0 and 180.0 Watts. Model NCR18650B from the manufacturer Panasonic was investigated with 10.0, 15.0, 28.0, 33.0, 39.0, 45.0, 55.0, 60.0, 64.0, 72.0 and 90.0 Watts, model IFR18650 from Shenzhen with 15, 22.0, 30.0, 45.0, 52.0, 60.0, 65.0, 70.0 and 75.0 Watts and model IMR18650 from Efest with 30.0, 50.0, 74.0, 111.0, 125.0, 135.0, 148.0, 158.0 and 170.0 Watts.

All models were tested to the minimum voltage of 0.00 Volts and the maximum voltage of 4.20 V; except model IFR18650, which has a maximum voltage of 3.65 V.

7.3. Accuracy estimation

The essential cell voltage range, relevant for the main measurement cycle results, is located between 1.00 V < = U < = 4.20 V. The test was carried out with the Bitrode test stand with a voltage measurement accuracy of ± 5 mV [18].

This amounted to a worst-case deviation of 0.5% at the minimum relevant voltage of 1.00 V. It was adopted that this has no significant influence on the measurement results and was therefore neglected.

The target was to examine the cell in a high-power range. Therefore, the most relevant measurements were performed in a power range

Table 5
Parameters used for cell aging checkups.

Boundary condition	Condition value	
Ambient temperature	25.0 °C	
Cell rest after measuring	At least 48 h	
State of charge (SOC)	100%	
Frequency range (EIS)	100 mHz–100 kHz	
Amplitude	100 mA	
Steps per decade	At lower limit	Above 66 Hz
	1	3
Measurement periods	At lower limit	Above 66 Hz
	3	10
Test method	Galvanostatic	

Table 6
Value deviation of the applied equipment [19].

Bitrode MCV4-100-5 CE [19]	Max. absolute deviation per channel	Max. accuracy per channel to full scale
Current	± 100 mA	± 0.1%
Voltage	± 5 mV	± 0.1%

Table 7
Worst case accuracies at the main power tests.

Battery Manufacturer/ Model	Absolute/relative time deviation	Absolute/relative energy deviation
LG/18650-HB6	16 s/1.7%	0.0892 Wh/1.7%
Panasonic/NCR18650B	139 s/3.5%	0.3858 Wh/3.5%
Shenzhen/ IFR18650	19 s/1.9%	0.0778 Wh/1.9%
Efest/ IMR18650	13 s/1.1%	0.1144 Wh/1.1%

$P >> 30.0$ W. Due to the cells internal resistance there was a voltage drop during discharge, the cell voltage during the power test was mainly $U < 3.60$ V, which resulted in a corresponding current of $I >> 8.0$ A. Therefore, the current accuracy ± 100 mA of the Bitrode test stand [19] resulted in a worst case deviation of 1.25% and is thus negligible for the usually higher power measurements (Table 6).

During test preparation, care was taken to ensure that the test channels were connected in parallel when currents close to 100.0 A were expected. Therefore, the measurement errors could be kept as small as possible.

The energy error was at a maximum at the smallest test current and was determined by the integral of the mean power deviation over time. The results are stated in Table 7.

8. Results and discussion

8.1. Prediction of constant power delivery

The following Figs. 4–7 display the measured data. All plots show the available discharging power as function of the discharge time. The measuring range of all specimens was from low to very high discharge loads:

From low to medium discharge loads, linear Peukert [7,9] behavior is observed, shown by the blue lines in the diagrams. At very high discharge rates an aberration from this behavior is observed. Less energy than predicted by the conversion of Peukert's law was found. This region is represented by the red lines in the diagrams (Figs. 4–7).

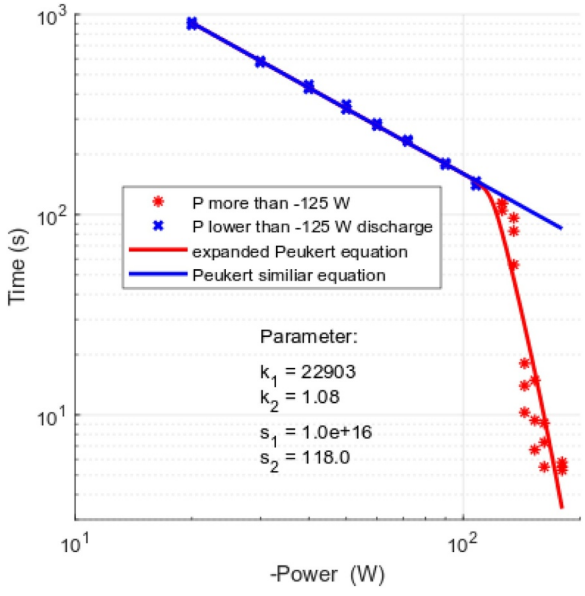

Fig. 4. LG Chem 18650-HB6.

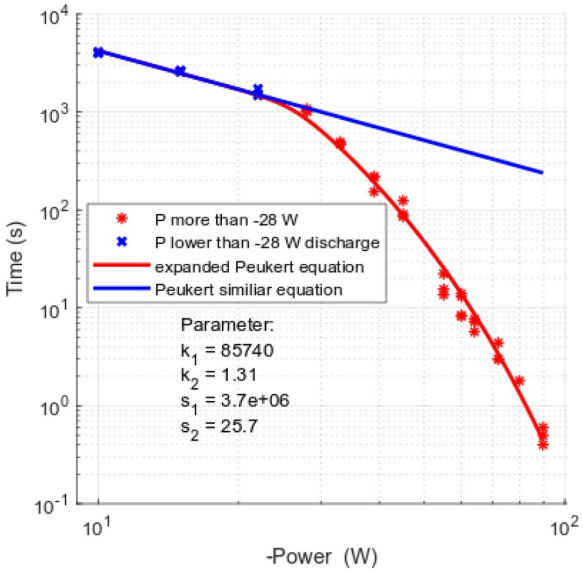

Fig. 5. Panasonic NCR18650B.

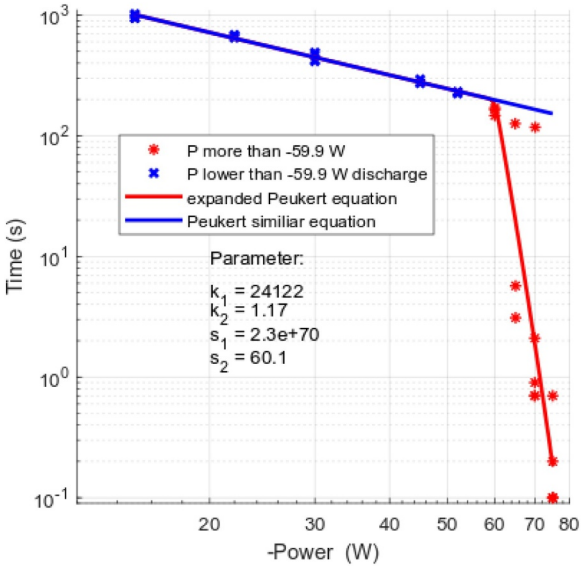

Fig. 6. Shenzhen IFR18650B.

8.2. Analysis

Data of four cylindrical 18650 lithium-ion cell types were evaluated. Figs. 4–7 display the fitting of the established correlation for each cell type.

Each graph compares the result of the energy/power Peukert's law (blue lines – low constant power loads) with the extended Peukert-bend equation (red lines – high constant power loads) for all examinees.

For calculation of the fitting parameters MATLAB R2018a was used, applying the least squares method which utilizes logarithmic error weighting. Table 8 summarizes the resulting fitting parameters k_1, k_2, s_1 and s_2 of the high-power behavior of the tested specimens presented in Figs. 4–7.

Parameter k_1 complies with the theoretical discharge energy at one watt, while k_2 correlates with the usual Peukert coefficient. s_2

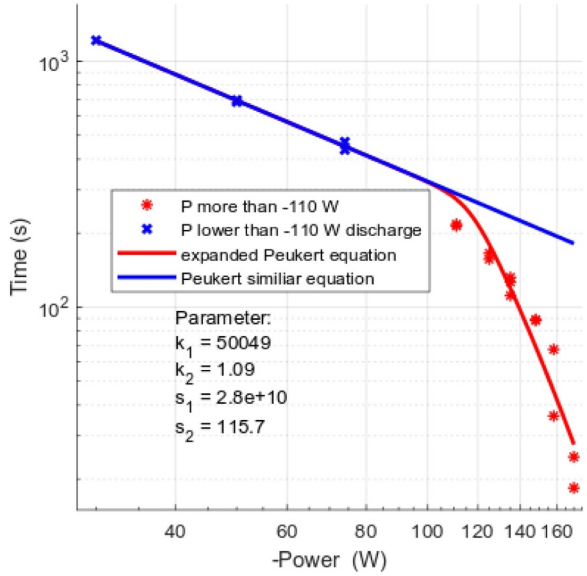

Fig. 7. Efest IMR18650.

Table 8
Fitting results.

Manufacturer/Model	k_1 in Wh	k_2	s_1	s_2 in W
LG/ 18650-HB6	6.362	1.08	$1.03 \cdot 10^{16}$	118.0
Panasonic/ NCR18650B	23.817	1.31	$3.66 \cdot 10^{6}$	25.7
Shenzhen/ IFR18650	6.701	1.17	$2.29 \cdot 10^{70}$	60.1
Efest/ IMR18650	13.903	1.09	$2.85 \cdot 10^{10}$	116.0

corresponds to the characteristic discharge load as threshold between the linear range (low constant discharge powers) and the non-linear section (high constant discharge powers). The parameter s_1 characterizes the power decrease in accordance with the occurring degradation at the high constant discharge powers for discharge powers higher than the value of parameter s_2.

9. Conclusion

In this work, the behavior of different lithium-ion cells at different constant power discharge rates was investigated. Normal operational power loads as well as power loads above the specifications of the cells were tested to see if there is a correlation. Based on the results of these measurements the correlation between the discharge power and discharge duration was investigated, similar to Peukert's law which states the correlation between discharge current and discharge duration. The key findings can be summarized as follows:

- Discharge of the cells with low to medium constant power resulted in a comparable correlation between discharge duration and discharge power as observed as Peukert's law which describes the correlation between discharge current and discharge duration.
- In the low to medium power region, a linear correlation between discharge power and duration was observed on a plot of discharge duration vs discharge power. This can be explained by introducing an intermediate voltage into the Peukert's law transferring it into an "energy/power" Peukert's law.
- The linear energy/power Peukert's law is no longer valid any upon the application of high constant power. Less discharge time is available as predicted with the linear equation. This observation is also similar to the reduction of discharge time vs. discharge current if constant current pulses were used, as described by Peukert's bend equation [9] described in literature.
- Similar to the low power region, the correlation between the discharge power and duration can be described by adding an intermediate voltage as an additional parameter into the Peukert bend equation.

The results of this study and the battery behavior revealed in this paper can provide better understanding to manufacturers and consumers of battery cells and systems about the dynamic behavior of their energy storage systems. The paper may provide guidelines to avoid over- or undersizing of batteries for energy storage systems utilized for high power loads. In the case of high and extreme power conditions, the results advise the duration for which the battery is able to deliver such loads, e.g. for boost power prediction of hybrid electric vehicles or for the design of overcurrent protection devices like fuses.

CRediT authorship contribution statement

Christoph Nebl: Conceptualization, Methodology, Software, Validation, Formal analysis, Investigation, Writing - original draft, Writing - review & editing, Visualization, Project administration, Funding acquisition. **Frank-Oliver Kotzur:** Conceptualization, Methodology, Software, Validation, Formal analysis, Investigation, Data curation, Visualization. **Daniel Koch:** Formal analysis, Writing - review & editing. **Hans-Georg Schweiger:** Conceptualization, Resources, Supervision, Project administration, Funding acquisition.

Declaration of Competing Interest

The authors declare that they have no known competing financial interests or personal relationships that could have appeared to influence the work reported in this paper.

Acknowledgments

The authors would like to thank Walter Straßer for all technical support and Francis Le Roux for correction and spell checking. The project upon which this publication is based was funded by the Federal Ministry of Education and Research under project numbers 16SBS018 (Schaufenster Elektromobilität) and 16PGF0166 (Post-Grant-Fund). The authors take responsibility for the content of this publication.

References

[1] M. Ringdorfer, M. Horn, "Development of a Wheel Slip Actuator Controller for Electric Vehicles using Energy Recuperation and Hydraulic Brake Control, Proceedings of IEEE International Conference on Control Applications, CCA, IEEE Multi-Conference on Systems and Control, MSC, 2011.
[2] C. Satzger, R. Castro, Predictive brake control for electric vehicles, IEEE Trans. Veh. Technol. 67 (2018) 977–990.
[3] S. Jones, E. Kural, K. Knödler, J. Steinmann, Optimal Energy efficiency, vehicle stability and safety on the OpEneR EV with electrified front and rear axles, Proceedings of International Forum on Advanced Microsystems for Automotive Applications, Berlin, 2013.
[4] A. Burke, M. Miller, The power capability of ultracapacitors and lithium batteries for electric and hybrid vehicle applications, J. Power Sources 196 (1) (2011) 514–522.
[5] M.E. Fuller, A battery model for constant-power discharge including rate effects, Energy Convers. Manag. 88 (2014) 199–205.
[6] S. Ioannou, K. Dalamagkidis, Runtime, capacity and discharge current relationshipf for lead acid and lithium batteries, Proceedings of 24th IEEE Mediterranean Conference on Control and Automation (MED16), Greece, 2016.
[7] W. Peukert, About the dependence of the capacity of the discharge current magnitude and lead acid batteries, Elektrotech. Z. 20 (1897) 287–288.
[8] D. Small, [Online]. Available: http://www.smartgauge.co.uk/peukert_depth.html, (March/2019), 2013.
[9] C. Nebl, F. Steger, H.G. Schweiger, Discharge capacity of energy storages as a function of the discharge current –expanding Peukert's equation, Int. J. Electrochem. Sci. 12 (2017) 4930–4957.
[10] Vötsch Industrietechnik GmbH, [Online]. Available: https://www.weiss-technik.com/de/marken/voetschtechnik/ (2019).
[11] LG Chem, Doc: BCY-PS-HB6-Rev1, Product Specification, Model: LG - 18650-HB6 1500mAh (2019).

[12] Panasonic Corporation Doc, Specifications, Model NCR18650B Doc: 2G23 × 0KYKU (2019).
[13] Shenzen Cottcell Battery Technology Co., Ltd, Specification, Model IFR18650 (2019).
[14] Efest Shenzhen Fest Technology Co., Ltd, Specification, Model IMR18650 (2018).
[15] Standard - IEC 61960:2011 (2011).
[16] Standard - ISO 12405-1:2011, (2011).
[17] S.R. Käbitz, Untersuchung der Alterung von Lithium-Ionen-Batterien mittels Elektroanalytik und elektrochemischer Impedanzspektroskopie, Rheinisch-Westfälischen Technischen Hochschule, Aachen, 2016 Dissertation.
[18] Zahner-Elektrik and Zahner-Schiller GmbH & Co. KG – Zahner Messysteme, [Online]. Available: http://zahner.de/products/electrochemistry/zennium.html, (2019).
[19] Bitrode Corporation, [Online]. Available: http://www.bitrode.com/model-mcv/, 2019.